Editors' Suggestion

Stochastic Processes in Magnetization Reversal Involving Domain-Wall Motion in Magnetic Memory Elements

Paul Bouquin,[1,2] Joo-Von Kim,[1] Olivier Bultynck,[2] Siddharth Rao,[2] Sebastien Couet,[2] Gouri Sankar Kar,[2] and Thibaut Devolder[1,*]

[1] *Université Paris-Saclay, CNRS, Centre de Nanosciences et de Nanotechnologies, Palaiseau 91120, France*

[2] *IMEC, Kapeldreef 75, Leuven B-3001, Belgium*

(Received 11 September 2020; revised 18 December 2020; accepted 12 January 2021; published 16 February 2021)

We show experimentally through single-shot time-resolved conductance measurements that magnetization reversal through domain-wall motion in sub-100-nm-diameter magnetic tunnel junctions is dominated by two distinct stochastic effects. The first involves the incubation delay related to domain-wall nucleation, while the second results from stochastic motion in the Walker regime. Micromagnetics simulations reveal several contributions to temporal pinning of the wall near the disk center, including vertical-Bloch-line nucleation and wall precession. We show that a reproducible ballistic motion is recovered when the Bloch and Néel wall profiles become degenerate in energy in optimally sized disks, which enables quasideterministic motion.

DOI: 10.1103/PhysRevApplied.15.024037

I. INTRODUCTION

The reversal of magnetization in nanostructures is a challenging problem for fundamental studies and technological applications. Beyond the coherent reversal mode in which all moments precess in unison as the magnetization switches, which is predicted [1–3] for lateral dimensions below approximately 25 nm but rarely observed in practice [4–6], the possibility of intermediate states involving nonuniform magnetic textures makes quantitative prediction of switching thresholds and durations a difficult task. The issue is exacerbated at finite temperatures, where thermal fluctuations render the reversal process stochastic. This is particularly problematic for information-storage applications, where deterministic switching is sought [7].

For perpendicularly magnetized thin-film disks with diameters greater than 25 nm, the reversal mode following the minimum energy path is predicted to involve the nucleation and propagation of a domain wall (DW) [8–12]. Such modes are therefore subject to stochastic effects in both the process of nucleation, which generally occurs at edge boundaries, and that of propagation, as the wall sweeps across the nanostructure. Since dipolar fields are nonuniform across such finite-sized systems, thermal fluctuations can induce a variety of phenomena that can transform the wall structure during reversal.

In this paper, we present experimental evidence of strong stochastic contributions to the free-layer reversal in circular magnetic tunnel junctions under spin-transfer torques (STTs, see Ref. [13]). Time-resolved measurements are interpreted with the aid of micromagnetics simulations and analytical modeling, which show that large-angle precession of the magnetization within the wall and the nucleation of vertical Bloch lines can contribute to the temporal pinning effects observed. We show how such effects can be mitigated when the Bloch and Néel wall structures become degenerate in energy; this suppresses most of the variability in the wall propagation dynamics.

II. EXPERIMENTAL METHODS

The devices studied are presented in Fig. 1(a): they are $Co_{20}Fe_{60}B_{20}$-MgO-based magnetic tunnel junctions (MTJs), with reference and hard layers organized in a standard synthetic antiferromagnet configuration. The MTJ switches by STT at zero field [Fig. 1(b)]. It is specifically optimized [14] to ensure easy DW propagation within the free layer. The primary requirement on the free-layer material is to avoid nonuniformities that would perturb the DW dynamics. The structural nonuniformities—potentially inducing pinning sites—are best avoided when the free layer growth can be really optimized because one is entirely free to choose the material buffer. Therefore, we use free layers embedded in top-pinned MTJs instead of bottom pinned MTJs. The nonuniformities can also arise from the nonuniform stray field of the reference layers of the MTJ. To minimize the detrimental effect of these unavoidably nonuniform [15] stray fields, we work with a free layer possessing a low moment (and hence a low Zeeman energy density) as well as a large thickness,

*thibaut.devolder@u-psud.fr

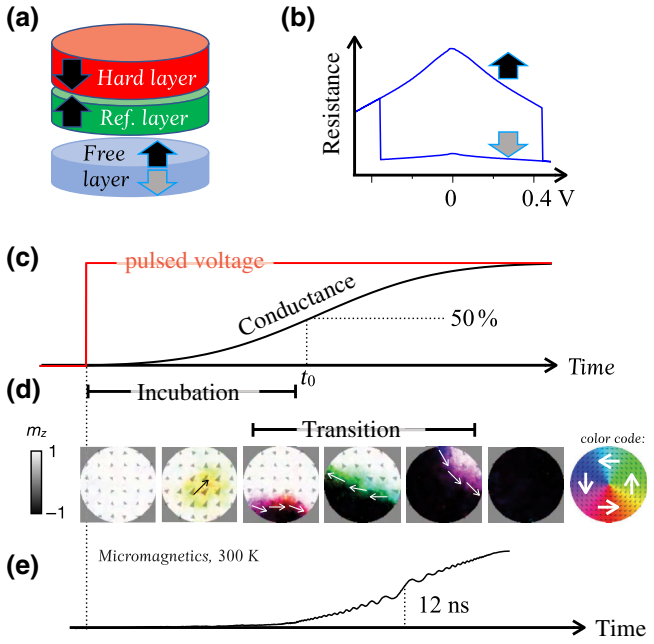

FIG. 1. (a) The device geometry. (b) The resistance versus voltage hysteresis loop. (c) A sketch of the experimental procedure. (d) Snapshots of some micromagnetic configurations during the simulated reversal of a 80-nm device at 300 K for a spin current of 5.4×10^{10} A/m^2. (e) The corresponding time-resolved magnetic moment.

which ends with a cap of 8Å of $Co_{20}Fe_{60}B_{20}$ in contact with the MgO tunnel oxide. These stringent requirements lead to MTJs that exhibit modest transport properties, with a magnetoresistance typically of 80% for a resistance-area product of RA = 9.6 $\Omega.\mu$m^2. In addition, the materials trade-offs made in order to achieve nice wall-propagative free layers lead to a reduced stability of the reference layers; this impedes a caveat-free experimental study of the parallel to antiparallel (P-to-AP) transition such that the experimental part of this paper focuses solely on AP-to-P switching. The experimental focus is on a device of diameter 100 nm, typical of the behavior in the interval of investigated sizes (70–100 nm).

Our setup applies fast-rising voltage steps with maximally flat plateaus and time resolves the device conductance [Fig. 1(c)] in a single-shot manner; the experimental configuration is very similar to that described in Ref. [16]. Note that the device impedances are much greater than the characteristic impedance of its surroundings, such that changes in the device conductance during switching do not change the applied voltage. The time-resolved conductance curves are thus illustrative of the device dynamics at constant applied voltage. In response to the voltage step, the device incubates during a variable delay and then its conductance changes abruptly. We fit the conductance waveforms with the ansatz $\mathrm{erf}[(t - t_0)/\tau]$ where erf is the standard error function to define an incubation delay t_0 and a transition time τ, which is thus the 24%–76% rise time. No correlation is ever detected between the incubation delays and the transition times. The micromagnetic simulations indicate that the transition corresponds to the sweeping of a DW through the device [Fig. 1(d)].

III. TIME-RESOLVED SWITCHING

Results from time-resolved switching are shown in Fig. 2. If the pulse polarity is chosen to induce the AP-to-P switching, the conductance first rises gradually in the

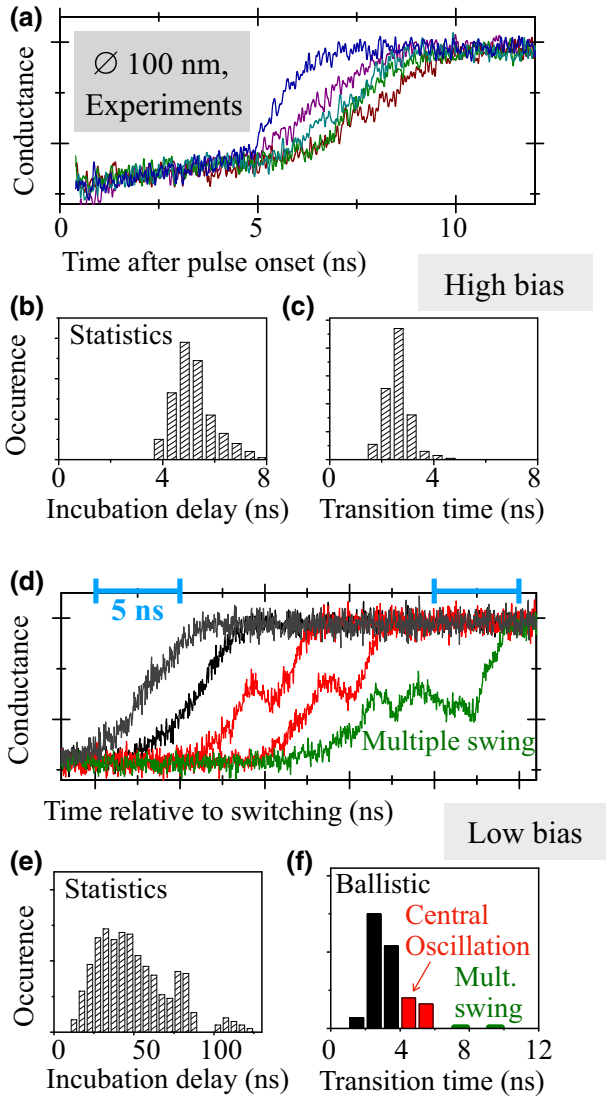

FIG. 2. The experimental signatures of the switching as a result of pulses of (a)–(c) 630 mV and (d)–(f) 500 mV on a 100-nm device. At low bias [panel (d)], the curves are horizontally offset to remove incubation delay t_0 and reveal the three classes of switching events: ballistic crossing of the midway conductance (black), crossing with one single pronounced oscillation (red), and multiple-swinglike crossing (green). (e),(f) The statistics of the incubation delay and transition time over 400 switching events; the two distributions show no correlation.

first 5 ns after the pulse onset. Experiments at lower voltage (not shown) indicate that, in fact, the conductance approaches asymptotically an on-current higher value, likely as a consequence of Joule heating. This interpretation is corroborated by the fact that no such conductance rise is observed for the other voltage polarity when the pulse is applied on the P state, the conductance of which is notably temperature independent. The subsequent time evolution of the conductance reflects the magnetic moment $\langle m_z \rangle$ of the free layer, with noticeable fluctuations of the incubation delay and of the transition time. Two distinct switching regimes are observed, depending on the magnitude of the STT. At high bias [Fig. 2(a)], the conductance waveforms are monotonic, with nanosecond-scale incubation delays and transition times. In the given example, the incubation lasts, on average, $\langle t_0 \rangle = 5.6$ ns and is slightly skewed to higher values [Fig. 2(b)]. Conversely, the distribution of transition times is rather symmetric about its average value $\langle \tau \rangle = 2.5$ ns [Fig. 2(c)].

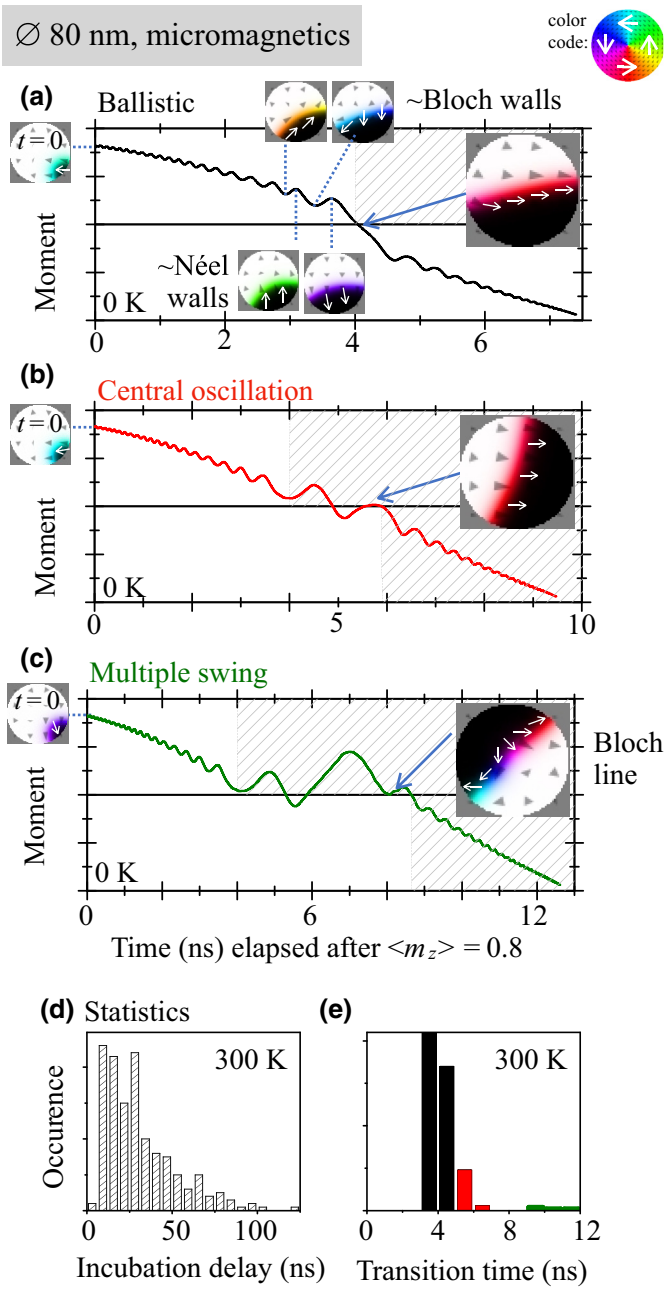

FIG. 3. The simulated DW dynamics within an 80-nm disk in a low-bias situation. (a)–(c) Examples of dynamics at $T = 0$ K for three initial states that differ only in the in-plane projection of the wall magnetization: the tilts at the wall centers are 90, 94, and 128°. The dashed areas underline the switching times; the white arrows sketch the magnetization direction within the wall. (d),(e) The statistics of the incubation delays and transition times for 300 switching simulations at $T = 300$ K at 3.5×10^{10} A/m^2.

When reducing the STT to just above the quasistatic switching threshold (low-bias regime), the dynamics slow down while getting more complex, particularly when the conductance is nearly midway between the initial and final states [Fig. 2(d)]. The distribution of transition times becomes asymmetric. Three types of switching events can be identified. In most events (black curves), the conductance still evolves monotonically, with transition times typically of 3–4 ns. We will see that these "ballistic" curves correspond to when the DW sweeps rather regularly through the device. For a fraction of events (20% probability, red curves), a pronounced oscillation is observed: the conductance first passes above the midway value and then it decreases for 1.3 ± 0.1 ns until it starts to rise again. The transition time is longer, typically 4–6 ns. We refer to these events as "central-oscillation" events, as we see that they arise when the wall oscillates once about the disk center. Finally, on rare occasions (approximately 2% probability, green curves) the midway conductance is crossed multiple times and τ exceeds 7 ns. These events are referred to as the "multiple-swing" ones, which occur when a 180° vertical Bloch line [17] appears in the wall while it is slow in the central region of the disk. These interpretations are based on the forthcoming micromagnetic simulations (Fig. 3).

IV. MICROMAGNETIC SIMULATIONS

Our simulations use the MuMax3 code, which solves the Landau-Lifshitz-Gilbert equation using the finite-difference method [18] with thermal fluctuations [19]. The $2R = 80$-nm diameter 2-nm-thick circular disk is discretized with $96 \times 96 \times 1$ cells, in a material [11] of magnetization $M_s = 1.2$ MA/m, exchange stiffness $A_{\mathrm{ex}} = 20$ pJ/m, perpendicular anisotropy constant $K_u = 1.18$ MJ/m^3, and damping $\alpha = 0.01$. The STT is accounted for by a symmetric Slonczewski term, where we assume unit spin polarization for simplicity.

A typical simulated reversal event at 300 K is presented in Fig. 1(d): it starts with the growth of a fluctuating "droplet" of precessing moments, which leads to nucleation of a 180° arclike curved wall when the

droplet encounters the disk edge. The in-plane magnetization within the wall is rather uniform. The wall then drifts across the device by a fast back-and-forth oscillatory motion that is reminiscent [20] of the wall precessional motion occurring above the Walker breakdown. As illustrated by the histograms of Figs. 3(e) and 2(f), the three categories of transition regime within the switching curves found experimentally are reproduced with similar probabilities in the simulations at 300 K—in contrast, the statistics of the incubation delay [Figs. 3(d) and 2(e)] cannot be well reproduced as the shortest time scales, likely because the device temperature is far from constant during the first few nanoseconds as a result of current-induced heating. Unfortunately, the corresponding micromagnetic configurations occurring once a wall is nucleated are comprised of a plethora of active fluctuators that conceal the intrinsic dynamics: on top of the wall motion, there is a breathing of its curvature and a nonuniform beating of its width, as well as ubiquitous short-range fluctuations. The physics of the transition is best revealed with $T = 0$ simulations of the wall dynamics. This requires properly chosen initial configurations in which the less relevant fluctuators are intentionally relaxed. We thus design empirically adequate initial states by numerically placing an optimally bent [9] wall near a disk edge. The wall is set with a uniform in-plane magnetization projection, qualitatively in line with the $T = 300$-K simulations.

Figures 3(a)–3(c) illustrate the possible motions of a wall at 0 K: while drifting, the wall acquires a straight shape when at the center and then bends again. Coincidentally with its velocity modulation, the wall passes periodically from the Bloch to the Néel configuration. Notably, it never crosses the center while in the pure Néel state. The oscillation of the moment is both more pronounced and slower when the wall approaches the disk center. Figures 3(a)–3(c) are meant to reveal how minute changes in the initial state alter the dynamics substantially when the wall later arrives in the center. Its motion can either be ballistic [Fig. 3(a)] or the wall can fail to cross the center at once. In this case, it withdraws before passing the center and resuming its oscillatory drift motion [Fig. 3(b)]. Alternatively, if choosing on purpose a specific initial tilt for which the wall happens to be maximally slow at the disk center, then the nonuniformity of the tilt can grow and lead to [inset in Fig. 3(c)] the creation of a vertical Bloch line [16]. Coincidentally, the DW swings multiple times in the central area, with a gyration move before finally passing.

V. COLLECTIVE COORDINATE MODEL FOR THE WALL PROPAGATION DYNAMICS

Further insight can be gleaned by an extension to the one-dimensional $\{q, \phi\}$ model [21] of the wall dynamics, where the motion is parametrized entirely by the position q of a straight wall and the internal wall angle ϕ (the "tilt"), which describes the chirality (Bloch or Néel) of the wall structure. The extension comprises accounting for the spatially nonuniform potential for the wall dynamics, which captures the fact that the disk center appears as an energy barrier to overcome, where the barrier height is related to the additional cost in DW energy required to extend it laterally across the disk. The equations of motion become

$$-\dot{\phi} + \alpha \frac{\dot{q}}{\Delta} = -\gamma_0 \left[H_d(q) + H_{\rm str}(q, \phi) \right], \tag{1}$$

$$\frac{\dot{q}}{\Delta} + \alpha \dot{\phi} = \gamma_0 \frac{H_{N \leftrightarrow B}}{2} \sin 2\phi + \sigma j, \tag{2}$$

where $\pi\Delta$ is the wall width and σj the magnitude of the STT [11]. H_d is the stray field of the two domains and $H_{N \leftrightarrow B}$ (typically 30 mT) is the in-plane field that would be needed to transform a Bloch DW into a Néel DW [22]. To describe the energy barrier in the q and ϕ directions, we define the two contributions to the wall stretch field:

$$H_{\rm str}(q,\ \phi) = \left(H_k^{\rm eff} + \frac{H_{N \leftrightarrow B}}{2} \cos^2 \phi \right) \frac{\Delta}{\ell_{\rm DW}} \frac{\partial \ell_{\rm DW}}{\partial q}, \tag{3}$$

where $\ell_{\rm DW}(q) = (1/\Delta) \int_{-R}^{R} dx\, {\rm sech}^2[(x-q)/\Delta] \sqrt{R^2 - q^2}$ is the effective length of the wall.

Figure 4(b) shows the phase portrait of the resulting wall trajectories in the (q, ϕ) space. The largely vertical flows, which take the wall from one disk edge to the other, remind us that the wall motion is in the Walker regime, since many oscillations of the wall tilt ϕ accompany the increase in q. The portrait also shows that the number of oscillations undergone by the wall is sensitive to the initial wall tilt. This sensitivity induces a stochasticity when the thermal fluctuations drive transitions between neighboring trajectories. Closer to the disk center, we observe that the Néel states ($\phi = 0[\pi]$) are associated with energy maxima, while the Bloch states ($\phi = \pi/2[\pi]$) give rise to saddle points. This representation shows that in addition to the "switching" trajectories (i.e., walls passing from one edge to the other) there is another family of trajectories. Indeed, if a Néel wall is placed at the center, it is transiently held there. It needs to spiral out of this energy maximum through a lossy back-and-forth transfer of energy between communicating vessels: the position degree of freedom of the wall and the tilt degree of freedom. The region in which walls of proper tilt are transiently pinned is a "retention pond," written as $\mathbb{P}$ and illustrated in Fig. 4(b). In the conservative limit, the spiraling-out trajectories inside the retention pond transform into closed circles; the half size of the pond $\mathbb{P}$ is then

$$\delta q_{\mathbb{P}} \approx R \sqrt{H_{N \leftrightarrow B} / H_{\rm k,eff}}. \tag{4}$$

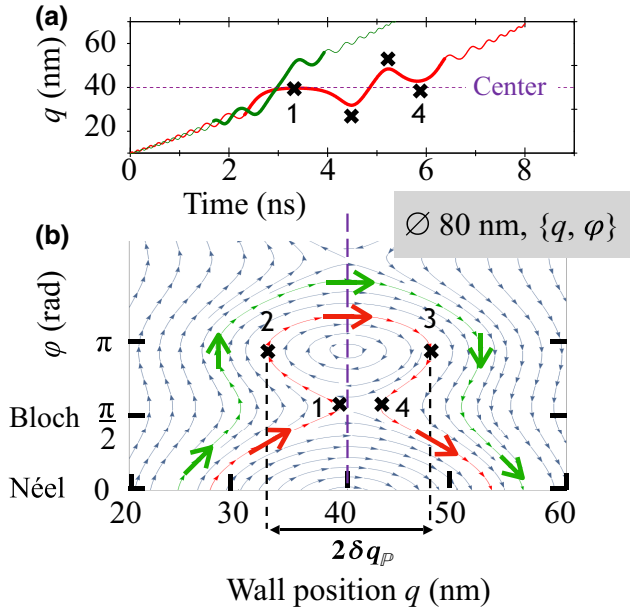

FIG. 4. The DW dynamics within a 80-nm disk in the $\{q, \phi\}$ model at low bias (4.5×10^{10} A/m^2). (a) Wall trajectories for walls initialized at $q = 10$ nm with initial tilts of 48° (green) and 91° (red). (b) Corresponding trajectories in the $\{q, \phi\}$ space. The red contour between the labels 1, 2, 3, and 4 is very close to the frontier of the retention pond $\mathbb{P}$.

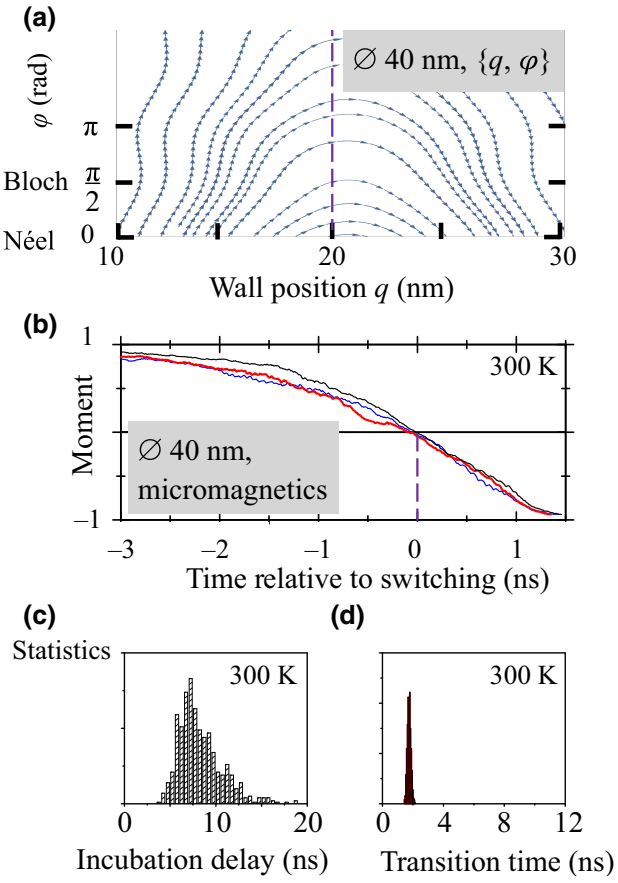

FIG. 5. The DW dynamics within a 40-nm disk at 5.4×10^{10} A/m^2. (a) The phase portrait of the wall trajectories within the $\{q, \phi\}$ model. (b) Three representative micromagnetic simulations at 300 K. (c),(d) Corresponding histograms of (c) the incubation delay and (d) the transition time.

VI. REPRODUCIBILITY OF THE TRANSITION TIME AND CONCLUSIONS

The concept of $\mathbb{P}$ is useful to understand the statistics of the transition time: the DW drift and its oscillation are rather independent phenomena, such that two situations can occur stochastically as a wall heads to the disk center. If the wall avoids the vicinity of $\mathbb{P}$ (green curve in Fig. 4), the $\{q, \phi\}$ model predicts a ballistic curve. If, in contrast, the wall happens to tangent the pond (red curve), it bypasses it by performing a back-and-forth motion with two pauses at either side near the disk center [positions 1 and 4 in Fig. 4(b)], in the formerly identified "central-oscillation" case. The $\{q, \phi\}$ models can thus explain some of the sensitivity to the tilt. However, since the $\{q, \phi\}$ model posits a uniform tilt, it cannot account for the multiple-swing trajectories that occur when the wall gets slow enough for a Bloch line to develop therein. The swinglike crossing can only be described using higher-dimensionality simulations such as in the micromagnetic ones or by using a more general collective coordinate model that would include a gradient of the tilt along the wall length. Despite its approximations, the (q, ϕ) model is illustrative, since it explains why the probability of nonballistic transition is correlated with the size of $\mathbb{P}$.

If one aims at a reproducible DW propagation while having no handle on the wall tilt, as in the presence of thermal noise, a solution is to find a geometry *without* a retention pond. In disks, there exists a single "magic" diameter for which the pond disappears and all wall trajectories are predicted to be ballistic, irrespective of the wall tilt. This happens when the energies of centered walls of Bloch or Néel characters are degenerate, i.e., when $H_{N \leftrightarrow B} = 0$. With our material parameters, this diameter is 40 nm [Fig. 5(a)]. One may object that this is not sufficient to guarantee reproducibility of the transition time, since the $\{q, \phi\}$ model posits a uniform tilt and hence cannot account for the rare "multiple-swing" trajectories that occur when the wall gets slow enough for a Bloch line to develop therein.

Fortunately, when using this diameter, the wall does not slow down near the disk center: this drastically reduces the probability that fluctuations can pile up and lead to the formation of a Bloch line within the wall. This optimistic conjecture is confirmed with micromagnetics [Figs. 5(b)–5(d)]. While the incubation delays are still distributed for a diameter of 40 nm, the transition regimes exhibit very little variance and the distribution

of the transition times is particularly narrow: the magic diameter ensures a repeatable wall motion independent of the tilt dynamics and immune from its fluctuations. If implemented jointly with the strategies ensuring reliable nucleation [23–26] and/or a reproducible wall tilt and wall position [27], this strategy opens up a route for reproducible switching times, which is of interest for memory applications in which write error rates could be substantially lowered.

ACKNOWLEDGMENT

This work was supported by the Interuniversity Microelectronics Centre (IMEC) Industrial Affiliation Program on spin-transfer torque–magnetic random-access memory (STT-MRAM) devices.

[1] J. Z. Sun, Spin-current interaction with a monodomain magnetic body: A model study, Phys. Rev. B **62**, 570 (2000).

[2] W. H. Butler, T. Mewes, C. K. A. Mewes, P. B. Visscher, W. H. Rippard, S. E. Russek, and R. Heindl, Switching distributions for perpendicular spin-torque devices within the macrospin approximation, IEEE Trans. Magn. **48**, 4684 (2012).

[3] H. Tomita, S. Miwa, T. Nozaki, S. Yamashita, T. Nagase, K. Nishiyama, E. Kitagawa, M. Yoshikawa, T. Daibou, M. Nagamine, T. Kishi, S. Ikegawa, N. Shimomura, H. Yoda, and Y. Suzuki, Unified understanding of both thermally assisted and precessional spin-transfer switching in perpendicularly magnetized giant magnetoresistive nanopillars, Appl. Phys. Lett. **102**, 042409 (2013).

[4] J. Z. Sun *et al.*, Spin-torque switching efficiency in CoFeB-MgO based tunnel junctions, Phys. Rev. B **88**, 104426 (2013).

[5] C. Hahn, G. Wolf, B. Kardasz, S. Watts, M. Pinarbasi, and A. D. Kent, Time-resolved studies of the spin-transfer reversal mechanism in perpendicularly magnetized magnetic tunnel junctions, Phys. Rev. B **94**, 214432 (2016).

[6] T. Devolder, A. Le Goff, and V. Nikitin, Size dependence of nanosecond-scale spin-torque switching in perpendicularly magnetized tunnel junctions, Phys. Rev. B **93**, 224432 (2016).

[7] A. V. Khvalkovskiy, D. Apalkov, S. Watts, R. Chepulskii, R. S. Beach, A. Ong, X. Tang, A. Driskill-Smith, W. H. Butler, P. B. Visscher, D. Lottis, E. Chen, V. Nikitin, and M. Krounbi, Basic principles of STT-MRAM cell operation in memory arrays, J. Phys. D: Appl. Phys. **46**, 074001 (2013), IOP Publishing.

[8] C.-Y. You, Switching current density reduction in perpendicular magnetic anisotropy spin transfer torque magnetic tunneling junctions, J. Appl. Phys. **115**, 043914 (2014).

[9] G. D. Chaves-O'Flynn, G. Wolf, J. Z. Sun, and A. D. Kent, Thermal Stability of Magnetic States in Circular Thin-Film Nanomagnets with Large Perpendicular Magnetic Anisotropy, Phys. Rev. Appl. **4**, 024010 (2015).

[10] J. Sampaio, A. V. Khvalkovskiy, M. Kuteifan, M. Cubukcu, D. Apalkov, V. Lomakin, V. Cros, and N. Reyren, Disruptive effect of Dzyaloshinskii-Moriya interaction on the magnetic memory cell performance, Appl. Phys. Lett. **108**, 112403 (2016).

[11] P. Bouquin, S. Rao, G. S. Kar, and T. Devolder, Size dependence of spin-torque switching in perpendicular magnetic tunnel junctions, Appl. Phys. Lett. **113**, 222408 (2018).

[12] L. Desplat and J.-V. Kim, Entropy-Reduced Retention Times in Magnetic Memory Elements: A Case of the Meyer-Neldel Compensation Rule, Phys. Rev. Lett. **125**, 107201 (2020).

[13] J. C. Slonczewski, Currents, torques, and polarization factors in magnetic tunnel junctions, Phys. Rev. B **71**, 024411 (2005).

[14] T. Devolder, J. V. Kim, J. Swerts, S. Couet, S. Rao, W. Kim, S. Mertens, G. Kar, and V. Nikitin, Material developments and domain wall-based nanosecond-scale switching process in perpendicularly magnetized STT-MRAM cells, IEEE Trans. Magn. **54**, 1 (2018).

[15] T. Devolder, R. Carpenter, S. Rao, W. Kim, S. Couet, J. Swerts, and G. S. Kar, Offset fields in perpendicularly magnetized tunnel junctions, J. Phys. D: Appl. Phys. **52**, 274001 (2019).

[16] T. Devolder, O. Bultynck, P. Bouquin, V. D. Nguyen, S. Rao, D. Wan, B. Sorée, I. P. Radu, G. S. Kar, and S. Couet, Back hopping in spin transfer torque switching of perpendicularly magnetized tunnel junctions, Phys. Rev. B **102**, 184406 (2020).

[17] V. Krizakova, J. P. Garcia, J. Vogel, N. Rougemaille, D. deSouza Chaves, S. Pizzini, and A. Thiaville, Study of the velocity plateau of Dzyaloshinskii domain walls, Phys. Rev. B **100**, 214404 (2019).

[18] A. Vansteenkiste, J. Leliaert, M. Dvornik, M. Helsen, F. Garcia-Sanchez, and B. V. Waeyenberge, The design and verification of MuMax3, AIP Adv. **4**, 107133 (2014).

[19] J. Leliaert, J. Mulkers, J. De Clercq, A. Coene, M. Dvornik, and B. Van Waeyenberge, Adaptively time stepping the stochastic Landau-Lifshitz-Gilbert equation at nonzero temperature: Implementation and validation in MuMax3, AIP Adv. **7**, 125010 (2017).

[20] T. Devolder, J.-V. Kim, F. Garcia-Sanchez, J. Swerts, W. Kim, S. Couet, G. Kar, and A. Furnemont, Time-resolved spin-torque switching in MgO-based perpendicularly magnetized tunnel junctions, Phys. Rev. B **93**, 024420 (2016).

[21] A. Thiaville, Y. Nakatani, J. Miltat, and N. Vernier, Domain wall motion by spin-polarized current: A micromagnetic study, J. Appl. Phys. **95**, 7049 (2004).

[22] A. Mougin, M. Cormier, J. P. Adam, P. J. Metaxas, and J. Ferré, Domain wall mobility, stability and walker breakdown in magnetic nanowires, Europhys. Lett. **78**, 57007 (2007).

[23] S. Pizzini, J. Vogel, S. Rohart, L. D. Buda-Prejbeanu, E. Jue, O. Boulle, I. M. Miron, C. K. Safeer, S. Auffret, G. Gaudin, and A. Thiaville, Chirality-Induced Asymmetric Magnetic Nucleation in Pt/Co/AlO_x Ultrathin Microstructures, Phys. Rev. Lett. **113**, 047203 (2014), American Physical Society.

[24] B. Lacoste, M. M. de Castro, T. Devolder, R. C. Sousa, L. D. Buda-Prejbeanu, S. Auffret, U. Ebels, C. Ducruet, I. L. Prejbeanu, L. Vila, B. Rodmacq, and B. Dieny, Modulating spin transfer torque switching dynamics with two

orthogonal spin-polarizers by varying the cell aspect ratio, Phys. Rev. B **90**, 224404 (2014).

[25] O. Bultynck, M. Manfrini, A. Vaysset, J. Swerts, C. J. Wilson, B. Soree, M. Heyns, D. Mocuta, I. P. Radu, and T. Devolder, Instant-On Spin Torque in Noncollinear Magnetic Tunnel Junctions, Phys. Rev. Appl **10**, 054028 (2018).

[26] S. Finizio, K. Zeissler, S. Wintz, S. Mayr, T. Weßels, A. J. Huxtable, G. Burnell, C. H. Marrows, and J. Raabe, Deterministic field-free skyrmion nucleation at a nanoengineered injector device, Nano Lett. **19**, 7246 (2019).

[27] M. Baumgartner, K. Garello, J. Mendil, C. O. Avci, E. Grimaldi, C. Murer, J. Feng, M. Gabureac, C. Stamm, Y. Acremann, S. Finizio, S. Wintz, J. Raabe, and P. Gambardella, Spatially and time-resolved magnetization dynamics driven by spin-orbit torques, Nat. Nanotechnol. **12**, 980 (2017), number: 10.